Generating Multicompartmental 3D Biological Constructs Interfaced through Sequential Injections in Microfluidic Devices

Giovanni Stefano Ugolini [1], Roberta Visone [1,2], Alberto Redaelli [1], Matteo Moretti [2,3,4,5], Marco Rasponi [1†]

Affiliations:

[1] Department of Electronics, Information and Bioengineering, Politecnico di Milano, Milano, Italy.

[2] Cell and Tissue Engineering Lab, IRCCS Istituto Ortopedico Galeazzi, Milano, Italy.

[3] Regenerative Medicine Technologies Lab, Ente Ospedaliero Cantonale, Lugano, Switzerland

[4] Swiss Institute for Regenerative Medicine, Lugano, Switzerland

[5] Cardiocentro Ticino, Lugano, Switzerland

[†]Corresponding author:

Marco Rasponi
Department of Electronics, Information and Bioengineering
Politecnico di Milano
Piazza Leonardo da Vinci 32
Building No. 21
20133 Milan, Italy
Email: marco.rasponi@polimi.it
Tel: +39 02 2399 3377

Abstract:

A novel technique is presented for molding and culturing composite 3D cellular constructs within microfluidic channels. The method is based on the use of removable molding PDMS inserts, which allow to selectively and incrementally generate composite 3D constructs featuring different cell types and/or biomaterials, with a high spatial control. We generated constructs made of either stacked hydrogels, with uniform horizontal interfaces, or flanked hydrogels with vertical interfaces. We also showed how this technique can be employed to create custom-shaped endothelial barriers and monolayers directly interfaced with 3D cellular constructs. This method dramatically improves the significance of *in vitro* 3D biological models, enhancing mimicry and enabling for controlled studies of complex biological districts.

I. COMMUNICATION

Increasing attention has been drawn in the last years towards the use of three-dimensional (3D) cell cultures as promising tools for expanding the relevance of *in vitro* biological models [1]. Hydrogel-based approaches have the advantage of providing improved mimicry of extra-cellular surroundings, since cells are embedded in matrices made of biopolymers such as collagen or fibrin[2,3]. The ability to culture 3D hydrogel-based cellular constructs within dedicated microfluidic devices represented a pivotal leap forward in the field, providing a high level of control on culture parameters (controlled supply and collection of culture media, application of physical stimuli, easy optical visualization) not otherwise achievable with macroscopic approaches [4–7]. Indeed, biological models of high relevance in the field of vascular [8–12], cardiac [13], liver [14] and brain [15] biology were produced by means of 3D cellular constructs cultured within microfluidic channels.

A large number of physiological structures, however, exhibit a compartmentalized morphology, characterized by geometrically organized architectures of different cell types or ECM materials (blood vessels, lung alveolar interface, osteochondral interface, blood-brain barrier, nephron units, gut epithelium, etc.) that are particularly challenging to model *in vitro*[16,17]. While 3D bio-printing represents a promising strategy for achieving fine geometrical control of biological *in vitro* constructs, it still requires costly equipment and suffers from technical limitations involving resolution, cell viability and compatibility with limited bioinks and low cell densities [18–22]. Microfabricated stamps have also proved able to transfer simple geometries to single [23] or multiple hydrogels [24]. In this last case, the use of thermo-responsive polymers and the limitation to agarose make the technology largely impractical in standard biological applications.

In general, all the above techniques are intrinsically limited as they cannot provide fluidic control to the biofabricated structures, a feature that would dramatically increase the

applications and relevance of *in vitro* multi-compartmental biological models. As for current microfluidic techniques, the spatial control of cell-laden hydrogels within microfluidic channels is still limited: cultures of multiple 3D hydrogels enclosed in a single channel can be attained by injecting hydrogels within confining structures (posts or pillars)[25] or by simultaneous injection of hydrogels with precisely controlled flowrates[26]. The latter strategy strictly depends on a complex and well-calibrated fluidic actuation apparatus and results impractical in standard laboratory use while the former strategy has the limitation of producing composite biological constructs obstructed by the presence of artificial confining structures. Such confining structures (typically PDMS pillars) have characteristic sizes of hundreds of microns and limit cellular contact interactions, paracrine interactions and the monitoring of cellular dynamics within the constructs, while adding undesired edge effects. The produced constructs therefore inevitably exhibit a worse mimicry of in vivo compartmental structures, characterized by continuous, unobstructed, interfaces. It is therefore not surprising that most advanced models of tissue-tissue interfaces still resort to 2D cell culture [27,28].

We here present a novel versatile technique for obtaining and culturing spatially controlled composite 3D cellular constructs within microfluidic channels. Figure 1 outlines the procedure by means of 3D sketches of a representative channel geometry. Two PDMS layers are fabricated through standard lithography techniques: a top culture layer comprising a microfluidic channel and four ports; a bottom molding layer designed to obtain a relief feature that partially interpenetrates the channel in the top layer (Figure 1A). After careful alignment, the two layers are brought into contact and the resulting PDMS device features a channel that is partially accessible for hydrogel injection from one of the ports. This is obtained thanks to the geometry of the bottom relief feature that allows to selectively and precisely occupy a portion of the top microfluidic channel. Upon hydrogel cross-linking, the

bottom molding layer is lifted and detached from the top culture layer. The hydrogel construct is retained in the top culture layer due to surface passivation of the bottom molding layer with bovine serum albumin. Lastly, the top layer is attached to a glass coverslip, thus allowing the injection of a second hydrogel in the remaining portion of the original channel (Figure 1B).

To culture the formed constructs under controlled conditions, we designed and fabricated top culture PDMS layers featuring a central channel and two side channels for culture medium supply. Depending on the bottom molding layer design, the final composite 3D constructs can be shaped according to custom-designed geometries. We designed layers aimed at culturing 3D constructs comprising two flanked cell-laden hydrogels (vertical interface, Layout 1) or two stacked cell-laden hydrogels (horizontal interface, Layout 2). Each configuration was exploited by combining two separate hydrogel solutions (fibrin and collagen gels) and embedding two populations of human primary bone marrow-derived mesenchymal stem cells (BM-MSC), tracked by means of different live cell dyes.

Figure 2 shows graphics of the employed microdevice geometries and target cross-sectional configurations of the composite 3D constructs (Figure 2A and 2E). In addition, confocal images of the cultured 3D constructs fixed both right after seeding and after 3 days of culture are presented to assess the spatial distribution of the cell-laden hydrogels forming the constructs. The seeding technique resulted efficient in forming 3D composite constructs made of two hydrogels embedding two cellular populations (red and green BM-MSC). As shown in Figure 2B and 2F, the constructs are highly homogenous with a uniform hydrogel interface along the whole length of the central channel. Detailed imaging of the constructs shows a uniform distribution of cells in the hydrogels forming the interface, both from a top view and along the constructs cross-section (Figure 2C and 2G). After 3 days of culture we observed cells migration and rearrangement, demonstrating continuity of the cellular

constructs (Figure 2D and 2H). We performed LIVE/DEAD assays on constructs formed through our novel technique with Layout 1 and 2 (Supplementary Material S1). Results confirm that a high cell viability is maintained, comparable to human BM-MSCs cultured on standard culture vessels. Moreover, no significant differences in cell viability are found between constructs formed with Layout 1 and 2 or between two compartments of Layout 1 constructs. To further prove the versatility of the proposed technique, we also cultured hybrid constructs seeded with two different hydrogel compositions (collagen-based hydrogels and fibrin-based hydrogels, Supplementary Material S2) demonstrating similar results in terms of construct homogeneity and interface uniformity. This demonstrates that complex organs-on-chip models can be formed with the present technique, where ECM materials are finely tuned to the biological compartment of interest and interfaced in composite constructs. Potential microfluidic models generated through geometries inspired to Layout 1 and 2 are particularly suited to bi-compartmental tissue structures such as osteo-chondral interface (cartilage, bone), musculoskeletal interface (muscle, tendons, bone), liver (hepato-biliary tract) and nephron compartments. Specifically, Layout 1 provides advantages in terms of imaging capabilities (interface interactions are clearly visible with standard microscopy) whereas Layout 2 may be advantageous for incorporating the constructs within multi-layer devices.

Physiological structures are often constituted by a cellular monolayer lining a 3D tissue. This is particularly true for endothelial or epithelial layers of blood vessels, intestinal or alveolar structures. Previous approaches aimed at interfacing endothelial monolayers with cell-laden 3D hydrogels are characterized by the obstructive presence of gel-confining posts [29]. In an attempt to explore the potential of the present microfluidic technique in forming 3D cell-laden constructs directly interfaced with endothelial monolayers, we designed two other layer geometries: one aimed at forming an endothelialized channel within a 3D cell-laden hydrogel (Layout 3) and one aimed at injecting two hydrogels in a central region and

allowing for endothelial monolayers to line the side media channels, forming an endothelial interface in direct contact with the vertical side surfaces of central cell-laden hydrogels (Layout 4). Since the scope of Layout 4 is related to the endothelial monolayer-hydrogel interface, we introduced a central array of posts in order to provide a means for performing two separate hydrogel injections (although that hydrogel-hydrogel interface is affected by the abovementioned limitations of confining structures) and provide structural support to a channel that could potentially sag due to high aspect ratio.

Figure 3 shows graphics of the employed layer geometries and target endothelialized 3D constructs (Figure 3A and 3B). In addition, confocal images of the cultured 3D constructs after 3 days of culture are presented to assess the extent and uniformity of endothelial cells layers (Figure 3C and 3D). A channel structure was effectively molded in cell-laden constructs cultured within the endothelialized channel microdevice configuration (Layout 3) as shown in top views and cross section of Figure 3E. Indeed, we injected cell suspensions of GFP-HUVECs and allowed for adhesion to the channel structure, demonstrating that the molded channel is pervious. Figure 3G shows 3D views of the construct after endothelialization: we observed a uniform monolayer of GFP-HUVECs lining the BM-MSC-laden channel structure. Images of constructs formed with GFP-HUVECs lining the side media channels (Layout 4) are shown in Figure 3F. The endothelium uniformly expressed endothelial marker CD31 throughout the covered surfaces of the media channels and the vertical surface of the cell-laden construct, as shown by high-magnification images (Supplementary Material S3). In addition, expression of VE-Cadherins localized on endothelial cells membrane confirms the structural junctions in the monolayer (Figure 3F). We conducted permeability assays to confirm the integrity of the endothelium: the endothelialized channels significantly hindered the diffusion of FITC-labelled 40kDa-dextran compared to control constructs without endothelialization. The average permeability

coefficient of the endothelial monolayer resulted to be $P_d = 3.60 \pm 2.08 \times 10^{-6}$ cm/s, which is in line with data from literature[8,10,30] (Supplementary Material S4). We therefore successfully obtained biologically-inspired configurations of functional endothelium-tissue interfaces with our novel microfluidic technique. Potential microfluidic models generated through geometries inspired to Layout 3 and 4 are particularly suited to studies of vascular-tissue interactions, blood-brain barrier, modeling of physiological/pathological cell extravasation dynamics, screening of compounds permeability through the endothelium towards a target tissue. Specifically, Layout 3 results oriented towards higher endothelium-tissue interaction, being the endothelial channel surrounded by the 3D cellular construct. On the other hand, Layout 4 features endothelial-tissue vertical walls, resulting more practical for directly assessing the mechanisms of molecule transport or cell migration through the layer.

In summary, we here described a novel microfluidics technique for molding and culturing 3D spatially-controlled composite constructs, made by different cell types and/or hydrogel formulations. By exploiting the reversible assembly of PDMS layers, we described for the first time how confining structures can be inserted and removed in microfluidic channels for multiple hydrogels injection. This process results particularly rapid and manageable if bottom layers are accurately designed to include features with sizes slightly smaller than those contained in top layers. In particular, with this gap (10 µm, Supplementary Figure S5), no leakage or hydrogel encroaching occurs by surface tension confinement. Molding of composite constructs is successfully achieved for features of approximately 200µm width, however, it is worth noting that resolution of this technique may vary depending on hydrogel chemistry and properties.

This method has the unique advantage of fabricating, directly within microfluidic environments, composite 3D cellular constructs where compartments are neatly interfaced in a wide variety of possible spatial architectures. We generated constructs made of stacked

cell-laden hydrogels featuring uniform horizontal interfaces with maximized surface of cell-cell interactions, a geometrical solution unattainable with previously described microfluidic methods. We also assembled 3D constructs with flanked hydrogels, forming a vertical interface, for easy visualization of interaction phenomena. We showed how this technique can be employed to create custom-shaped endothelial barriers and monolayers directly interfaced with 3D cellular constructs. Based on simple injections in microfluidic channels, this methodology overcomes some bioprinting limitations as it shows high resolution, high versatility towards different hydrogels or high cell densities and, most importantly, it adds tunable microfluidic control to the biofabricated structures. Future technical challenges include the combination of neat, pillar-free multi-compartmental constructs directly interfaced with endothelial monolayers. Perspective biological applications involve the development of organs-on-chips where fluidically controlled 3D multi-cellular and multi-ECM *in vitro* constructs are oriented at an improved modeling and mimicking of biological structures such as blood-brain barrier, blood vessels, osteochondral interface, gut and alveolar interfaces. Given the complexity of *in vivo* biological architectures of tissues and organs, this method paves the way to a dramatic increase in the similarity of *in vitro* 3D biologically-inspired constructs to complex and compartmentalized biological structures.

II. Experimental procedures

A. Microdevices design and master molds fabrication

Microdevice designs were drawn through standard CAD software (AutoCAD, AutoDesk Inc., USA). Transparency masks were printed at high-resolution (64'000 dpi) and used as photomasks for fabrication of master mold through SU-8 (SU8-2100, SU8-2050, MicroChem, USA) photolithography. Features height was set as follows: 200µm for top culture channels of all microdevice configurations and for bottom molding relief features of

vertical interface device (Layout 1) and side endothelium devices (Layout 4); 100μm for bottom molding relief features of other microdevice configurations (Layout 2, 3). Bottom layer designs were drawn to obtain relief features slightly smaller than the top culture channels. To this aim, a lateral gap of 10μm between bottom molding layer features and top culture channels was employed that did not induce hydrogel leaking nor affected the injection. Supplementary Figure S5 highlights the lateral gaps for two representative device layouts (Layout 1 and 2). This strategy was employed to favor interpenetration and ease the process of alignment, however, it resulted also possible to assemble and operate layers designed without lateral gaps. PDMS layers were fabricated by replica molding of PDMS (Sylgard 184, Dow Corning, Germany. 10:1 mixing ratio) on master molds. Channel inlets and outlets were created by punching 1mm (for hydrogel injection channels) and 5mm (for media channels) through-holes on top layers only.

B. Cell extraction and culture

Human primary BM-MSC were isolated from bone marrow aspirates obtained from patients during routine orthopedic surgical procedures and after obtaining written informed consent. Cells were expanded and cultured in a humidified incubator at 37°C, 5% CO_2 at all stages. Culture medium employed had the following composition: alpha-modified Eagle's medium supplemented with 10% fetal bovine serum (FBS), 10mM HEPES, 1mM sodium pyruvate, 100U/mL penicillin, 100μg/mL streptomycin and 300μg/mL L-glutamine (ThermoFisher, Italy), supplemented with 5 ng/mL of fibroblast growth factor-2 (Peprotech, UK). At passage number 6, two cell populations were incubated with two different Vybrant cell labeling solutions (ThermoFisher, Italy. DiO and DiI dyes) and then detached from culture flasks for seeding experiments.

GFP-expressing HUVECs were purchased from Lonza and cultured in EGM-2 Bullet-kit medium (Lonza, Italy). Cells were used for experiments at passage number 3.

C. Microdevice assembly and seeding procedure

PDMS layers were sterilized by UV irradiation. Bottom layers were coated with 3% bovine serum albumin (BSA, Sigma, Italy) to prevent hydrogel adhesion and then carefully aligned and assembled to the top layers. Fibrin gels were formed by mixing fibrinogen and thrombin solutions (Sigma, Italy) to obtain the following final concentrations: 20 mg/ml fibrinogen, 2U/ml thrombin, 10^7 cells/ml. Rat tail type I collagen (Sigma, Italy) was used to prepare collagen gels with final concentrations of 3 mg/ml collagen neutralized with 1M NaOH to 7.2-7.4 pH and embedding 10^7 cells/ml. Cell-laden hydrogels were injected in the gel inlets of the microdevices and allowed to cross-link in humidified chambers placed in standard cell culture incubators for 3' (fibrin gels) or 30' (collagen gels).

After cross-linking, bottom layers were gently detached from top layers, quickly brought into contact with a sterile coverslip and a second hydrogel embedding cells labeled with a different dye was injected. Subsequent to hydrogel cross-linking, culture medium was injected in the media channels. For endothelialization experiments, GFP-HUVECs were suspended in EGM-2 medium at a concentration of $5x10^6$ cells/ml. After top layers assembly with coverslips, the cell solution was either injected directly in the molded channel (Layout 3) or pipetted in the wells of the media channels (Layout 4) pre-loaded with 30µl of EGM-2 medium. GFP-HUVECs were allowed to adhere for 1 hour before adding additional culture medium to the wells. Cells were statically cultured with medium changing operations performed every 24 hours. The seeding procedure for a representative device (Layout 1) is demonstrated in the Supplementary Movie 1.

D. Immunofluorescence and image acquisition

Microdevices were fixed for 20' with 4% paraformaldehyde. For immunofluorescence stainings, cells were permeabilized with 0.1% Triton-X and blocked with 3% BSA. Cells were probed with mouse anti-human primary antibodies (VE-Cadherin and CD31, Immunotech., USA) and goat anti-mouse rhodamine-conjugated seconday antibodies (Sigma, Italy). Image acquisition was performed with a Olympus FluoView FV10i confocal microscope. Images were taken at either 10X or 60X magnification, with approximate z-axis resolution of 12μm and 1μm respectively. Image processing and 3D reconstructions were performed with ImageJ software (National Institute of Health, USA).

References:

[1] M. Ravi, V. Paramesh, S. R. Kaviya, E. Anuradha, F. D. Paul Solomon, *J. Cell. Physiol.* **2015**, *230*, 16.

[2] M. W. Tibbitt, K. S. Anseth, *Biotechnol. Bioeng.* **2009**, *103*, 655.

[3] A. Khademhosseini, R. Langer, *Biomaterials* **2007**, *28*, 5087.

[4] D. Huh, G. A. Hamilton, D. E. Ingber, *Trends Cell Biol.* **2011**, *21*, 745.

[5] V. van Duinen, S. J. Trietsch, J. Joore, P. Vulto, T. Hankemeier, *Curr Opin Biotechnol* **2015**, *35*, 118.

[6] G. Y. Huang, L. H. Zhou, Q. C. Zhang, Y. M. Chen, W. Sun, F. Xu, T. J. Lu, *Biofabrication* **2011**, *3*, 12001.

[7] X. Zhang, L. Li, C. Luo, *Lab Chip* **2016**, *16*, 1757.

[8] J. S. Jeon, S. Bersini, M. Gilardi, G. Dubini, J. L. Charest, M. Moretti, R. D. Kamm, *Proc. Natl. Acad. Sci. U. S. A.* **2014**, *112*, 214.

[9] S. Kim, H. Lee, M. Chung, N. L. Jeon, *Lab Chip* **2013**, *13*, 1489.

[10] I. K. Zervantonakis, S. K. Hughes-Alford, J. L. Charest, J. S. Condeelis, F. B. Gertler, R. D. Kamm, *Proc. Natl. Acad. Sci. U. S. A.* **2012**, *109*, 13515.

[11] L. L. Bischel, E. W. K. Young, B. R. Mader, D. J. Beebe, *Biomaterials* **2013**, *34*, 1471.

[12] J. A. Whisler, M. B. Chen, R. D. Kamm, *Tissue Eng. Part C. Methods* **2014**, *20*, 543.

[13] A. Marsano, C. Conficconi, M. Lemme, P. Occhetta, E. Gaudiello, E. Votta, G. Cerino, A. Redaelli, M. Rasponi, *Lab Chip* **2016**, *16*, 599.

[14] Y.-C. Toh, T. C. Lim, D. Tai, G. Xiao, D. van Noort, H. Yu, *Lab Chip* **2009**, *9*, 2026.

[15] J. D. Wang, E. S. Khafagy, K. Khanafer, S. Takayama, M. E. H. Elsayed, *Mol. Pharm.* **2016**, *13*, 895.

[16] K. Yum, S. G. Hong, K. E. Healy, L. P. Lee, *Biotechnol. J.* **2014**, *9*, 16.

[17] D. Huh, Y. Torisawa, G. a. Hamilton, H. J. Kim, D. E. Ingber, *Lab Chip* **2012**, *12*, 2156.

[18] S. V Murphy, A. Atala, *Nat. Biotechnol.* **2014**, *32*, 773.

[19] F. Pati, J. Gantelius, H. A. Svahn, *Angew. Chemie Int. Ed.* **2016**, *55*, 4650.

[20] S. Q. Chang, B. Kang, Y. D. Dai, H. X. Zhang, D. Chen, *Nanoscale Res Lett* **2011**, *6*, 591.

[21] H. Lee, D.-W. Cho, *Lab Chip* **2016**, *16*, 2618.

[22] L. Yang, S. V. Shridhar, M. Gerwitz, P. Soman, *Biofabrication* **2016**, *8*, 35015.

[23] M. D. Tang, A. P. Golden, J. Tien, *J. Am. Chem. Soc.* **2003**, *125*, 12988.

[24] H. Tekin, T. Tsinman, J. G. Sanchez, B. J. Jones, G. Camci-Unal, J. W. Nichol, R. Langer, A. Khademhosseini, *J. Am. Chem. Soc.* **2011**, *133*, 12944.

[25] C. P. Huang, J. Lu, H. Seon, A. P. Lee, L. a Flanagan, H.-Y. Kim, A. J. Putnam, N. L. Jeon, *Lab Chip* **2009**, *9*, 1740.

[26] A. P. Wong, R. Perez-Castillejos, J. C. Love, G. M. Whitesides, *Biomaterials* **2008**, *29*, 1853.

[27] D. Huh, B. D. Matthews, A. Mammoto, M. Montoya-Zavala, H. Y. Hsin, D. E. Ingber, *Science* **2010**, *328*, 1662.

[28] H. J. Kim, D. Huh, G. Hamilton, D. E. Ingber, *Lab Chip* **2012**, *12*, 2165.

[29] S. Chung, R. Sudo, I. K. Zervantonakis, T. Rimchala, R. D. Kamm, *Adv. Mater.* **2009**, *21*, 4863.

[30] J. S. Jeon, I. K. Zervantonakis, S. Chung, R. D. Kamm, J. L. Charest, *PLoS One* **2013**, *8*, e56910.

Tables and Figure Legends

Figure 1 – Overview of the composite 3D constructs seeding technique, outlined for a representative channel geometry. Insets show 2D cross sections of microdevice components. A) PDMS layers employed in the constructs molding procedure: a top PDMS culture layer, a bottom PDMS molding layer and a glass coverslip. B) Seeding procedure: after careful alignment of top and bottom PDMS layers (i), the top culture layer is only partially accessible and injected with a first hydrogel solution (ii). Upon hydrogel cross-linking, the bottom layer is detached from the top culture layer (iii) and discarded. The top layer enclosing the cell-laden hydrogel is transferred onto a glass coverslip (iv) thus making accessible the remaining part of the top culture layer channel. A second cell-laden hydrogel is then injected and allowed to cross-link (v).

Figure 2 – Composite 3D cellular constructs obtained with two layers geometries for molding flanked hydrogels (vertical interface) or stacked hydrogels (horizontal interface). A) Assembly of PDMS layers for forming flanked composites (Layout 1). Inset shows the desired final construct configuration with two side-by-side hydrogels. B) Overview of the entire flanked 3D composite construct both in phase contrast imaging and in fluorescent imaging showing two cell-laden fibrin hydrogels (red and green). C) Detailed images of a representative flanked composite 3D construct fixed right after seeding. Top views (phase contrast and fluorescence) show a precise spatial localization of the two cell-laden fibrin hydrogels with a uniform distribution of the two cell populations (red and green stained BM-MSCs). A representative side view image demonstrates uniformity also along the cross-section of the construct. D) Detailed images of a representative flanked composite 3D construct fixed after 3 days of culture. Top views (phase contrast and fluorescence) and cross section (fluorescence imaging) show cell interactions and co-localization taking place nearby the fibrin hydrogels interface. E) Assembly of microdevice layers for forming stacked composites (Layout 2). Inset shows the desired final construct configuration with two stacked hydrogels. F) Overview of the entire stacked composite 3D construct both in phase contrast imaging and in fluorescent imaging showing two cell-laden fibrin hydrogels (red and green). G) Detailed images of a representative stacked composite 3D construct fixed right after seeding. A representative cross-section of the construct shows a precise stacked distribution of the two cell-laden hydrogels with a uniform distribution of the two cell populations (red and green BM-MSCs). H) Detailed images of a representative stacked composite 3D

construct fixed after 3 days of culture demonstrating that stacked hydrogels distribution is maintained over time.

Figure 3 – Composite 3D cellular constructs obtained in endothelialization experiments. A) Assembly of PDMS layers for forming perfusable endothelialized channels (Layout 3). Inset shows the desired final construct configuration with endothelial cells lining a channel structure molded in a cell-laden fibrin hydrogel. B) Assembly of PDMS layers for forming side endothelium lining the vertical surfaces of a cell-laden hydrogel (Layout 4). Inset shows the desired final construct configuration with two cell-laden hydrogels and endothelial cells seeded in side media channels, lining the vertical surfaces of the gels. C) Overview of the Layout 3 construct. D) Overview of the Layout 4 construct. E) Detailed images of a representative 3D construct with a molded channel fixed after 3 days of culture with and without addition of GFP-HUVECs. Without HUVECs: Top views (phase contrast and fluorescent images) and cross-section (fluorescent image only) show a uniform channel shape molded in the cell-laden fibrin hydrogel. BM-MSCs are represented in red. With HUVECs: a cross-section and a longitudinal 3D portion of the endothelialized channel molded in the cell-laden 3D construct (bottom). GFP-HUVECs (green) uniformly line the inner surface of the channel structure. F) Detailed images of a representative 3D construct with endothelium lining the side vertical surfaces of cell-laden fibrin hydrogels fixed after 3 days of culture. 3D views show the endothelium formation on the vertical surface of the 3D construct (BM-MSCs represented in red while GFP-HUVECs are represented in green) and a high-magnification detail of HUVECs on the bottom surface and vertical hydrogel surface expressing membrane-localized VE-Cadherin (DAPI, blue; VE-Cadherin, yellow).

Figures

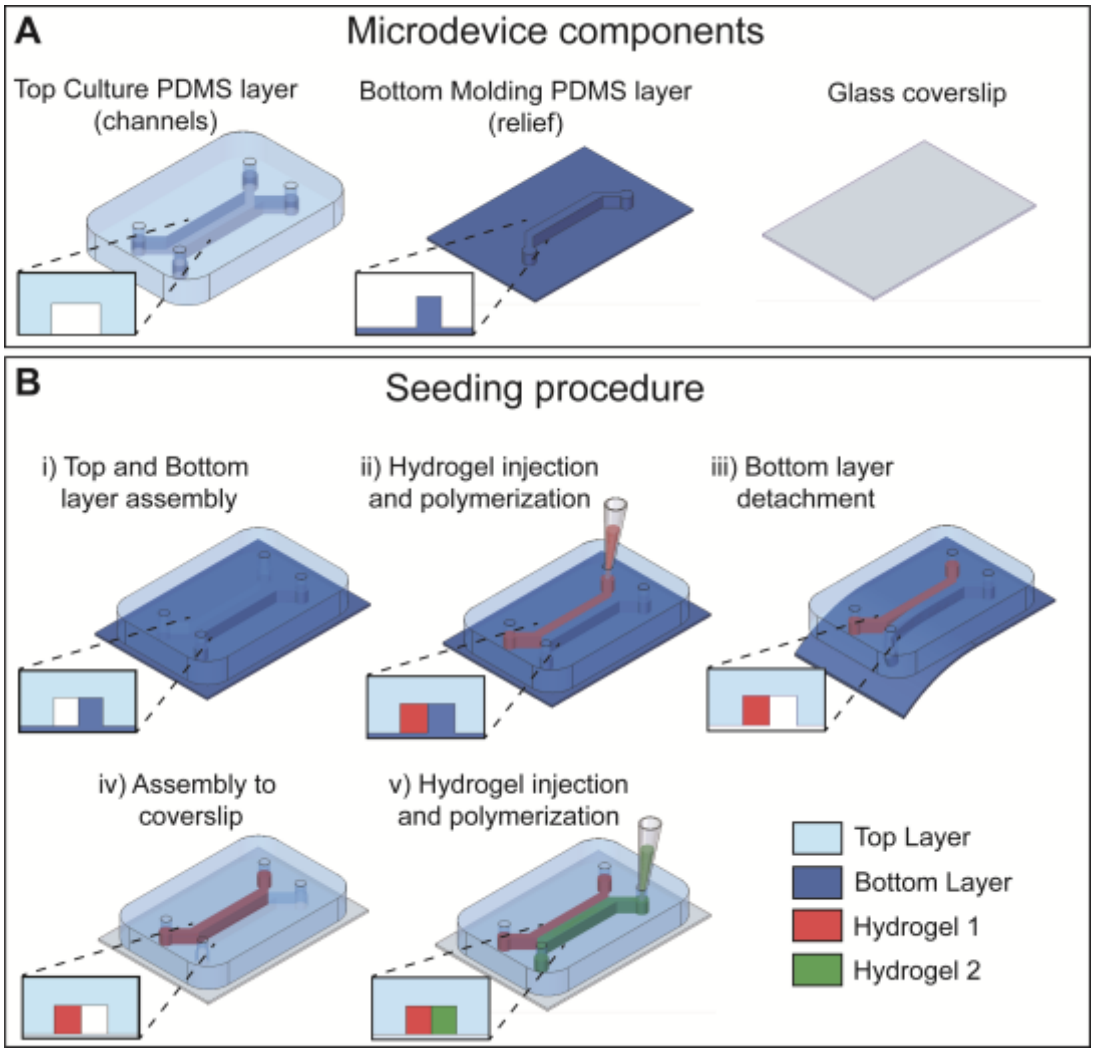

Figure 1

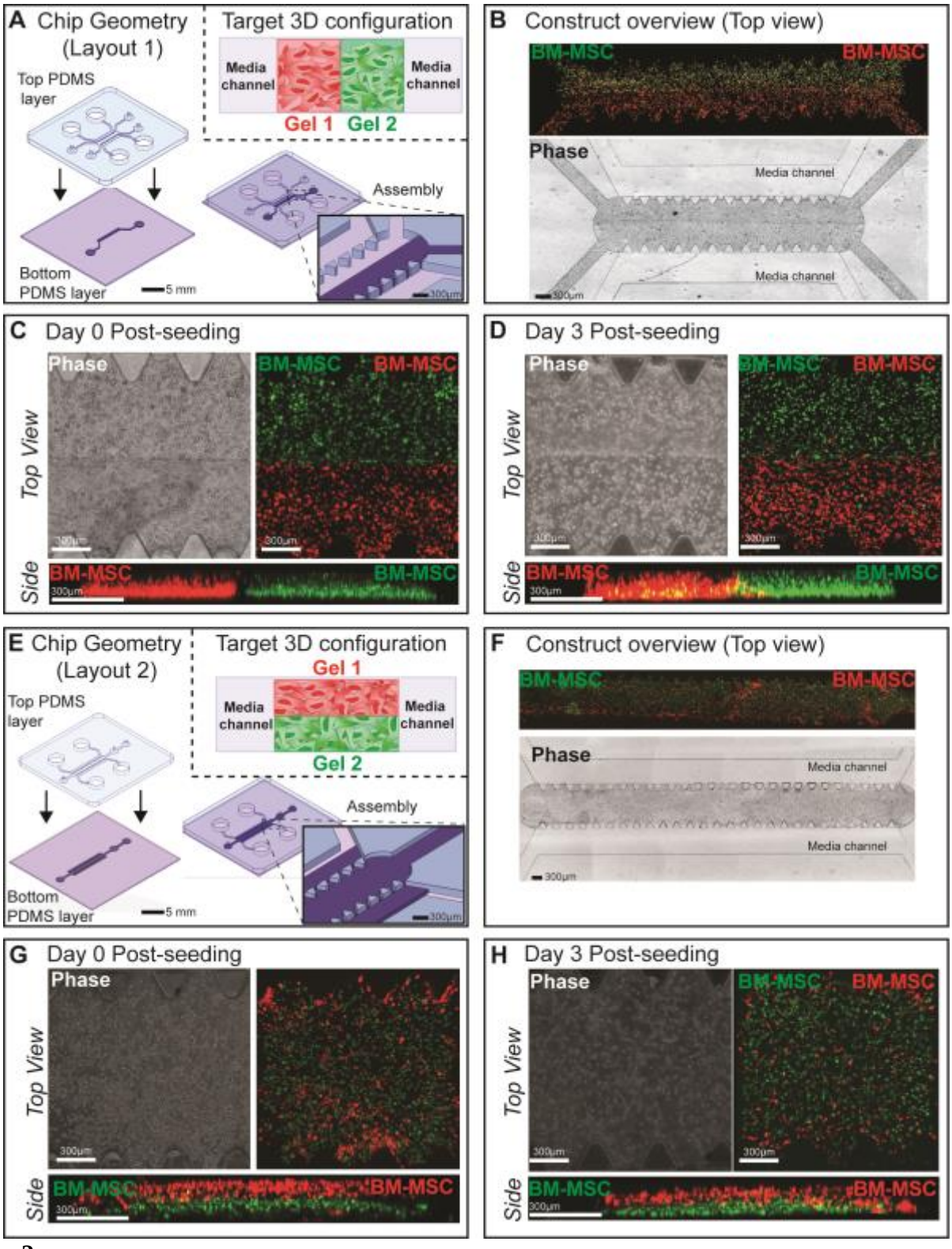
A Chip Geometry (Layout 1)
Target 3D configuration
Media channel
Media channel
Gel 1
Gel 2
Top PDMS layer
Assembly
Bottom PDMS layer
5 mm
B Construct overview (Top view)
BM-MSC
BM-MSC
Phase
Media channel
Media channel
C Day 0 Post-seeding
Phase
BM-MSC
BM-MSC
Top View
Side
BM-MSC
BM-MSC
D Day 3 Post-seeding
Phase
BM-MSC
BM-MSC
Top View
Side
BM-MSC
BM-MSC
E Chip Geometry (Layout 2)
Target 3D configuration
Gel 1
Media channel
Media channel
Gel 2
Top PDMS layer
Assembly
Bottom PDMS layer
5 mm
F Construct overview (Top view)
BM-MSC
BM-MSC
Phase
Media channel
Media channel
G Day 0 Post-seeding
Phase
Top View
Side
BM-MSC
BM-MSC
H Day 3 Post-seeding
Phase
BM-MSC
BM-MSC
Top View
Side
BM-MSC
BM-MSC

Figure 2

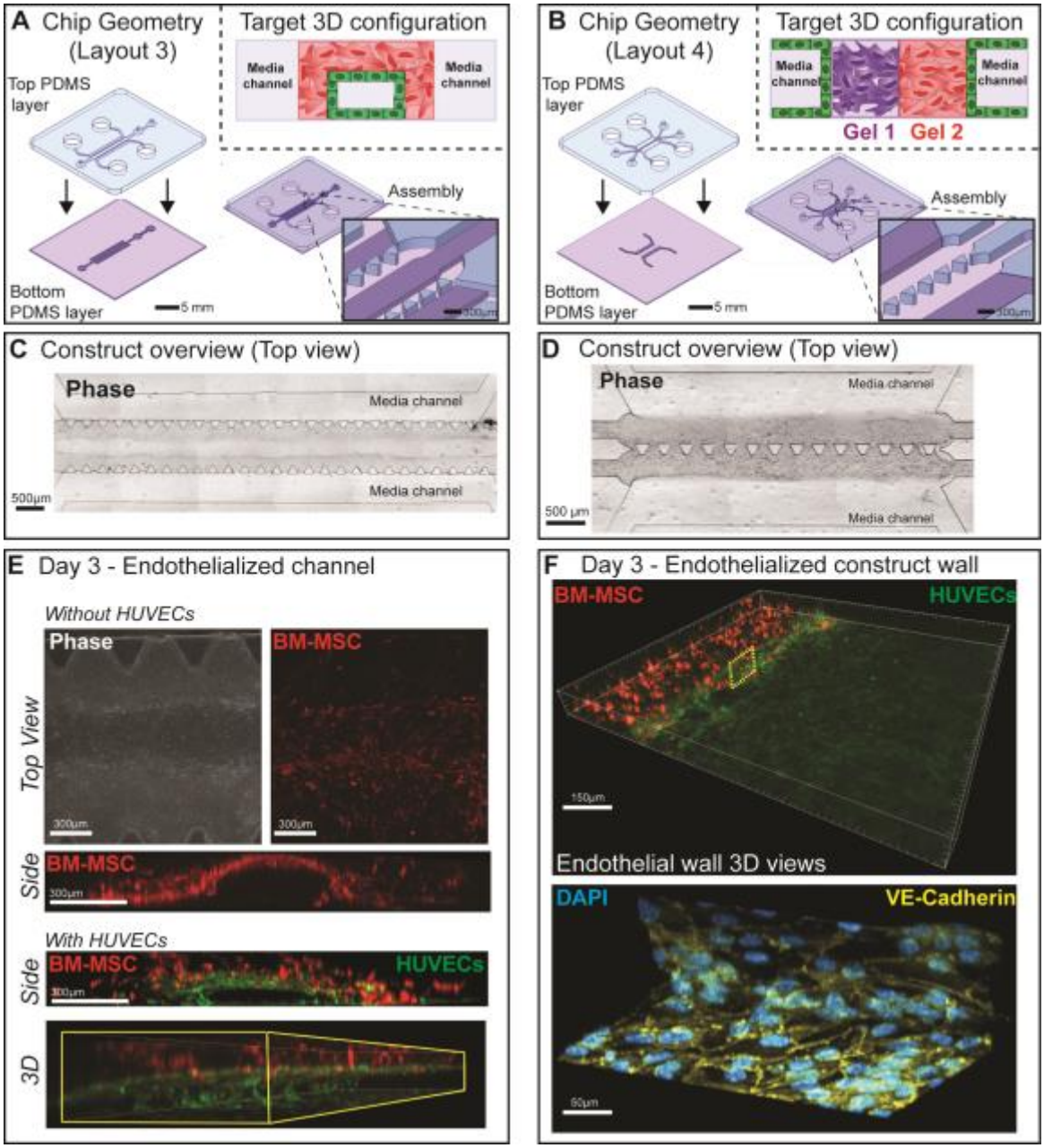
A Chip Geometry (Layout 3)
Target 3D configuration
Media channel
Media channel
Top PDMS layer
Assembly
Bottom PDMS layer
5 mm
B Chip Geometry (Layout 4)
Target 3D configuration
Media channel
Media channel
Gel 1
Gel 2
Top PDMS layer
Assembly
Bottom PDMS layer
5 mm
C Construct overview (Top view)
Phase
Media channel
Media channel
500µm
D Construct overview (Top view)
Phase
Media channel
Media channel
500 µm
E Day 3 - Endothelialized channel
Without HUVECs
Top View
Phase
BM-MSC
300µm
300µm
Side
BM-MSC
300µm
With HUVECs
Side
BM-MSC
HUVECs
3D
F Day 3 - Endothelialized construct wall
BM-MSC
HUVECs
150µm
Endothelial wall 3D views
DAPI
VE-Cadherin
50µm

Figure 3